

Unidirectional, Ultrafast, and Bright Spontaneous Emission Source Enabled By a Hybrid Plasmonic Nanoantenna

Guoce Yang, Qixin Shen, Yijie Niu, Hong Wei, Benfeng Bai,* Maiken H. Mikkelsen,* and Hong-Bo Sun

Inefficient and wide-angle emission as well as low emission rate of optical nanoemitters (such as quantum dots) have been strongly limiting their practical applications in next-generation nanophotonic devices, such as nanoscale light-emitting diodes (LEDs) and on-chip single photon sources. Optical nanoantennas provide a promising way to deal with these challenges. Yet, there has been no solution that can overcome these drawbacks simultaneously on a single device. Here, a hybrid plasmonic nanoantenna consisting of a silver nanocube positioned at the center of a gold concentric-ring structure is proposed, which can simultaneously enhance the emission directionality and decay rate of quantum dots embedded in the nanogap beneath the nanocube while maintaining high quantum efficiency. Coupling quantum dots to this nanoantenna can result in 60% of the emitted photons collected by the first lens with a numerical aperture (NA) of 0.5 and 21% for a NA of 0.12. The total emission intensity and decay rate are enhanced by 121-fold and 424-fold, respectively, compared with quantum dots on a glass substrate. A high quantum efficiency above 50% is obtained in simulation. This novel platform can be applied to enhance various types of optical nanoemitters and to develop high-speed directional nano-LEDs and single photon sources.

level, which limits the speed of optical devices that are needed in next-generation optical interconnect and quantum communication, such as high-speed nanoscale light emitting diodes (LEDs)^[8] and single photon sources.^[9] Directional and high speed nano-LEDs can potentially be used in data centers to reduce the energy consumption.^[10] On-demand single photon sources with high emission rate and good directionality can attain high repetition rate and near-unity collection efficiency.^[11] In addition, the omnidirectional far-field spontaneous emission from nanoemitters can be collected by using antenna structures and high numerical aperture (NA) optics.^[12] But the collection efficiency of emitted photons directly into low NA optics, such as a single mode fiber, is quite low, which hinders the on-chip integration. Thus, the poor emission directionality and long lifetime (corresponding to the slow decay) are two main challenges for practical applications based on

spontaneous emission. The use of plasmonic nanoantennas with nanocavities^[13] is one of the most effective solutions to obtain ultrafast spontaneous emission due to their ability to extremely localize and enhance the photon density of states, which in turn results in enhanced spontaneous emission^[14,15] due to the Purcell effect.^[16] On the other hand, an optical antenna is able to couple the emitted light into the antenna modes and then reradiate photons into specific spatial directions.

1. Introduction

Typical optical nanoemitters such as organic molecules,^[1,2] semiconductor quantum dots,^[3,4] solid state defects,^[5] and 2D materials^[6,7] are playing fundamental roles in the field of nanophotonics and quantum technology. However, the intrinsic lifetime of spontaneous emission is usually on nanosecond


Dr. G. Yang, Prof. B. Bai, Prof. H.-B. Sun
State Key Laboratory of Precision Measurement and Technology
Department of Precision Instrument
Tsinghua University
Beijing 100084, China
E-mail: baijenfeng@tsinghua.edu.cn

Dr. G. Yang, Prof. M. H. Mikkelsen
Department of Electrical and Computer Engineering
Duke University
Durham, NC 27708, USA
E-mail: m.mikkelsen@duke.edu

Q. Shen, Prof. M. H. Mikkelsen
Department of Physics
Duke University
Durham, NC 27708, USA

Y. Niu, Prof. H. Wei
Beijing National Laboratory for Condensed Matter Physics
Institute of Physics, Chinese Academy of Sciences
Beijing 100190, China

Y. Niu
School of Physics and Technology
Wuhan University
Wuhan 430072, China

 The ORCID identification number(s) for the author(s) of this article can be found under <https://doi.org/10.1002/lpor.201900213>

DOI: 10.1002/lpor.201900213

In order to realize highly directional emission, there have been some antenna designs, such as the Yagi–Uda antenna,^[17–19] the split ring resonator,^[20] the concentric-ring structure,^[21–24] the hexagonal array,^[25] and the metal nanowire.^[26] By comparison, the concentric-ring structure, namely the bullseye antenna, has exhibited superior emission directionality normal to the ground plane due to its circular symmetry. Good emission directionality has been experimentally obtained for various quantum emitters coupled to bullseye antenna, such as fluorescent molecules,^[21] quantum dots,^[27–29] and nitrogen-vacancy centers.^[30,31] However, only modest emission rate can be obtained in such structures.^[31] To accelerate the spontaneous decay process, a plasmonic nanogap, as a typical plasmonic nanocavity, is an ideal choice to increase the photon density of states by confining light into a small nanoscale volume. Typical examples include the bowtie antenna^[32] and nanodimer antenna^[33] as the representatives of horizontal nanogaps, and the nanopatch antennas as the representatives of vertical nanogaps.^[34] The latter can sharply enhance the Purcell factor, that is, the figure of merit of the decay rate enhancement.^[35] But the broad far field radiation pattern^[15] still limits the collection efficiency of radiated light into low NA optics. So far, there has been no design featuring both remarkable lifetime reduction and directivity enhancement. Therefore, the hybridization of plasmonic nanocavity and bullseye nanoantenna provides an achievable solution to meet both requirements.

In this work, a film-coupled nanocube is integrated into a bullseye antenna, forming a cube-bullseye hybrid plasmonic nanoantenna. It can utilize the advantages of both structures to enhance the spontaneous decay rate of quantum dots and obtain high directionality of emission in the direction normal to the ground plane. We experimentally demonstrate that the hybrid plasmonic nanoantenna can dramatically shorten the lifetime of quantum dots fluorescence by a factor of 420 and enhance the intensity by 120 times, by referring to quantum dots on glass substrates. Meanwhile, 60% and 21% of the emitted photons can be collected by optical systems with NAs of 0.5 and 0.12, respectively, which are the typical NAs of a multimode fiber and a single-mode fiber.

2. Results and Discussion

A 3D schematic of the proposed nanoantenna is shown in **Figure 1a**. This hybrid plasmonic antenna consists of gold concentric rings on a gold film (i.e., the bullseye structure) and a silver nanocube at the center. The period, width, and height of the rings are 560 nm, 280 nm and 50 nm, respectively. CdSe/ZnS core–shell quantum dots (whose emission wavelength is 640 nm in water solution) are filled in the nanogap between the silver nanocube and the ground gold film, where gap plasmon resonance can happen. The plasmonic nanogap performs like a nanocavity that can confine light into an extremely small mode volume and thus can lead to large Purcell enhancement and increased quantum efficiency by tuning the cavity resonance to the emission wavelength. The resonance wavelength depends on both the nanocube size and the gap thickness that is mainly determined by the size of quantum dots (≈ 10 nm). The colloidal quantum dots were characterized by transmission electron microscopy

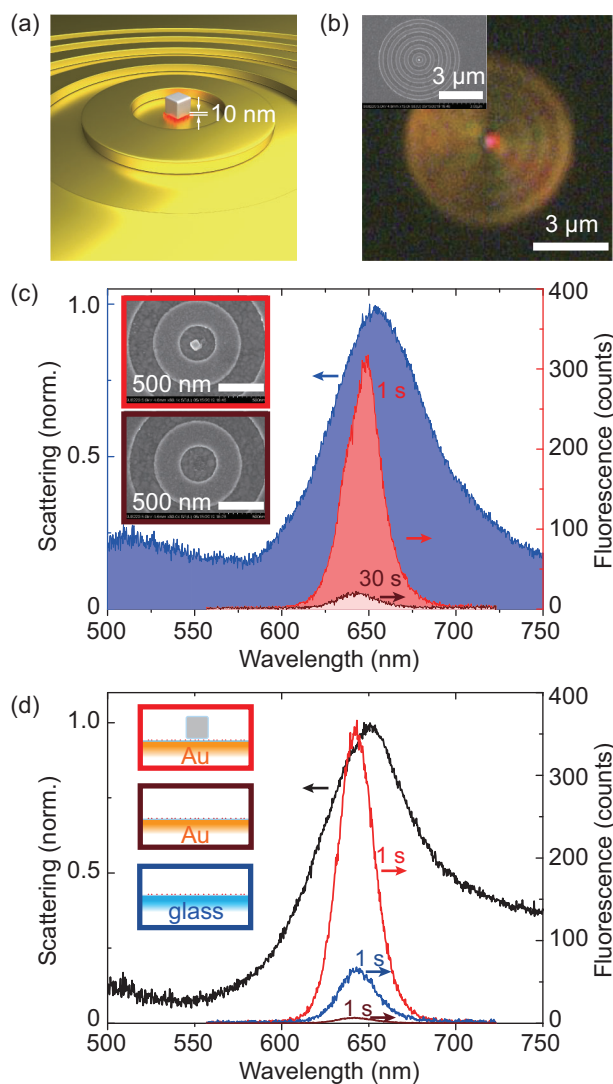


Figure 1. The cube-bullseye hybrid plasmonic nanoantenna and the measured spectra. a) 3D illustration of the hybrid plasmonic nanoantenna consisting of gold concentric rings on a gold film and a silver nanocube situated at the center of the rings. The nanocube and the gold film are separated by a monolayer of CdSe/ZnS quantum dots with diameter of ≈ 10 nm. b) Dark-field image of the hybrid plasmonic antenna, where the red spot at the center corresponds to the scattering of the nanocube positioned at the center; inset: SEM image of the cube-bullseye hybrid plasmonic antenna. c) Blue: the scattering spectrum of the cube-bullseye hybrid plasmonic antenna; Red: the fluorescence spectrum from quantum dots coupled to the fabricated hybrid plasmonic antenna using an exposure time of 1 s; Brown: the fluorescence spectrum from a gold bullseye structure without the silver cube using an exposure time of 30 s; inset: SEM images of the fabricated antennas with (red box) and without (brown box) a silver nanocube at the center of the gold rings. d) The fluorescence spectra from different reference samples of quantum dots on glass (blue), on bare gold film (brown), and in the nanogap between the silver nanocube and the gold film (red), using the exposure time of 1 s. The measured scattering spectrum of the silver nanocube is shown as the black curve, whose resonance wavelength matches the emission wavelength of quantum dots.

(Figure S2a, Supporting Information). Here, 90-nm-sized monodispersed colloidal silver nanocubes were chosen to keep the resonant wavelength at around 650 nm. Two-step electron beam lithography and lift-off process were employed to fabricate the hybrid nanoantenna (see Supporting Information). A red light spot, due to the scattering of the film-coupled nanocube, can be evidently seen at the center of the structure in the dark-field microscopic image (Figure 1b). The spot and the corresponding scattering spectrum (blue spectrum in Figure 1c) clearly show that the cube is well positioned at the center of the rings and the gap resonance matches well with the emission wavelength of the quantum dots. The scanning electron microscopy (SEM) images of the samples are shown in the insets of Figures 1b,c. On the one hand, the monolayer quantum dots can be seen at the center of the bullseye structure in the SEM image (see the inset in the brown box in Figure 1c); on the other hand, the resonant wavelength also indicates the gap thickness of ≈ 10 nm. Actually, two or more layers of quantum dots would make the nanogap thicker (>20 nm) and the strongly blue shift of the resonant wavelength. The number of quantum dots in the nanogap is estimated around 40 by considering the density of quantum dots and the size of the nanocube. The photoluminescence (PL) emission peak from the sample is at the wavelength of 650 nm (see the red spectrum in Figure 1c), which is very close to the original emission wavelength of the colloidal quantum dots on glass (see the blue curve in Figure 1d). The PL spectrum from a sample without the silver cube was also measured (see the brown spectrum in Figure 1c). The emission intensity is 16 times weaker even if a 30 times longer exposure time was used. The measured fluorescence spectrum reveals a 480-fold PL intensity enhancement. Note that the SEM characterization was performed after all the optical measurements had been done. The PL spectra from monolayered quantum dots on bare gold film, on glass substrate, and embedded in the gap of a single film-coupled nanocube are also shown in Figure 1d. All the PL spectra in Figure 1c,d were obtained using an excitation power density of ≈ 20 W cm $^{-2}$ at the wavelength of 532 nm. It is seen that the PL intensity from quantum dots coupled to the cube-bullseye hybrid antenna (red curve in Figure 1c) is much larger than those of quantum dots on glass (blue curve in Figure 1d) and on bare gold film (brown curve in Figure 1d). A 121-fold enhancement (compared with quantum dots on glass) can be calculated with an area-normalized factor defined below.

$$\langle EF \rangle = \frac{I/A_{\text{cube}}}{I_{\text{glass}}/A_{\text{spot}}} \quad (1)$$

where I is the measured PL intensity from the antenna sample, I_{glass} is the PL intensity from the glass sample, A_{cube} is the projection area of the nanocube, and A_{spot} is the laser spot area with diameter of ≈ 500 nm.

For a single film-coupled nanocube, the emission from the quantum dots located in the nanogap not only results in the far field radiation into free space but also launches the surface plasmon polaritons (SPPs) at the interface between the gold film and air. The electric field distribution under a vertically oriented electric dipole calculated by 3D full-wave simulation (using COMSOL Multiphysics) demonstrates the SPP mode on the surface of the gold film (Figure 2a). The energy of SPPs completely

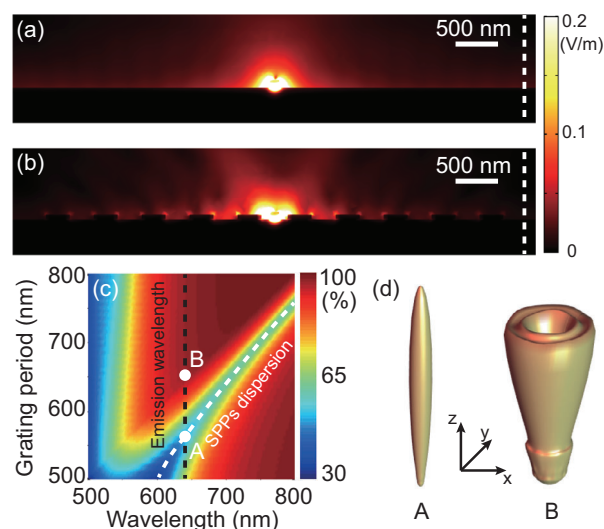


Figure 2. SPPs coupling mechanism for the directional emission. a) Simulated cross-sectional electric field distribution in a single film-coupled silver nanocube in absence of the bullseye structure, which is excited by a vertically oriented electric dipole beneath the right corner of the nanocube for maximum coupling to the gap mode. The propagation of SPPs along the gold film surface is observed. b) Simulated cross-sectional electric field distribution in the proposed cube-bullseye hybrid plasmonic antenna excited by a vertically oriented electric dipole underneath the right corner of the nanocube, which shows the interaction between the circular grating and the SPPs. c) Simulated reflectance spectrum of a linear strip gold grating on the gold film (with strip height 50 nm and filling factor of 50%) under normal incidence. The absorption band spanning from the wavelengths of 600 nm to 800 nm indicates the SPP mode. The absorption around the wavelength of 500 nm is due to the inter-band transition of gold. White dashed line: dispersion curve of the SPPs; Black dashed line: emission wavelength of the quantum dots. d) Simulated far-field emission patterns from quantum dots coupled to cube-bullseye hybrid plasmonic antennas with two different periods of A) 560 nm and B) 650 nm, corresponding to point A (on SPP resonance) and point B (off SPP resonance), respectively, marked in (c).

dissipates during the propagation due to the Ohmic loss in the metal if there is no other structure on the gold film. However, the existence of the bullseye structure can modify the propagation of the SPPs. The simulated electric field shows that the amplitude of the electric field at a lateral distance 3 μ m away from the center (shown by the white dashed line) at the gold–air interface is half of that at the same location in the absence of the bullseye structure (Figure 2a,b), which indicates that the SPPs are partially decoupled into the upper space by the bullseye structure during the propagation. The interaction between the bullseye structure and the SPPs excited by the quantum dots emission can lead to directional emission. When the phase matching condition $\beta_{\text{spp}}(\lambda) = 2\pi/\Lambda$ is satisfied (where β_{spp} is the propagation constant of SPPs, λ is the wavelength of light in vacuum, and Λ is the circular grating period), the SPPs are coherently scattered by the circular grating structure and the interference leads to the wave propagation to the free space along the direction normal to the ground plane.

For a given wavelength, there exists an optimal grating period. To optimize the grating period and simplify the calculation, a 1D linear grating, consisting of periodic gold strips on a gold ground substrate, is studied because it is a good approximation along

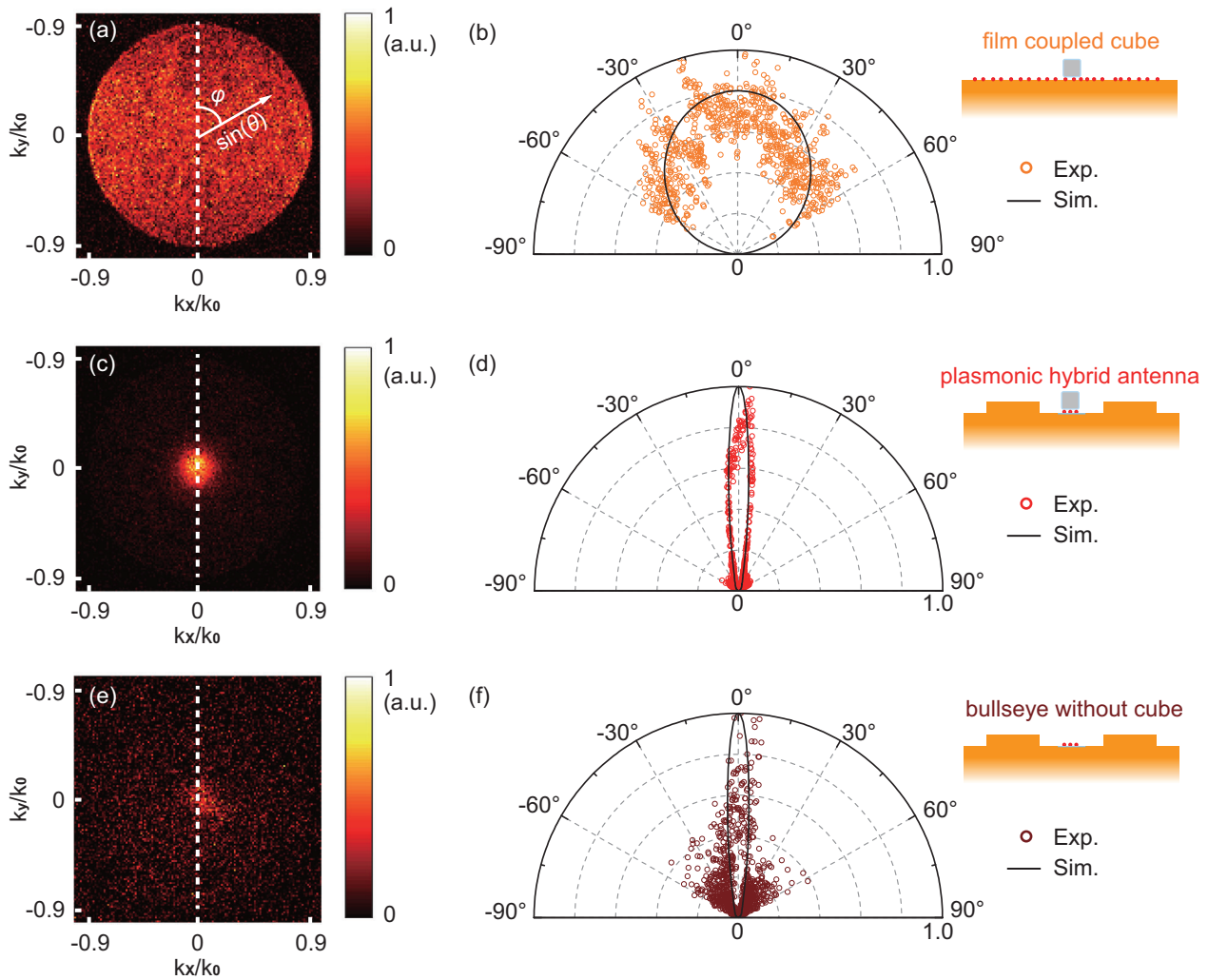


Figure 3. Far-field emission patterns of the quantum dots. a,c,e) Measured k -space images and b,d,f) retrieved 2D angular far-field emission patterns of quantum dots coupled to a single film-coupled nanocube without rings (top row), a cube-bullseye hybrid plasmonic antenna (middle row), and a bullseye structure without cube (bottom row). The angular patterns are retrieved along the white dashed lines (polar angle $\varphi = 0^\circ$) in (a), (c) and (e), where the azimuthal angles are retrieved by $\theta = \sin^{-1}(k_y/k_0)$.

the radial direction of the bullseye structure. The reflectance spectrum as a function of the period and wavelength is calculated and shown in Figure 2c, where the reflection dip implies the energy dissipation at the resonant wavelength of SPPs. According to the phase matching condition, the optimal grating period should be equal to the SPPs wavelength that is shorter than the counterpart in vacuum. The relationship between the period and the resonant wavelength due to SPPs is also clearly indicated by the white dashed SPP dispersion curve in Figure 2c. The emission wavelength of the quantum dots used in this work is also marked as the black dashed line in Figure 2c. The cross point A between the emission line and the SPPs dispersion curve determines the optimal period of 560 nm, where the SPP resonance band overlaps well with the quantum dots emission band. The point B on the black dashed line in Figure 2c corresponds to a non-optimal period of 650 nm. 3D full-wave simulations and a subsequent near-field to far-field transformation^[36] were used to calculate the 3D far-field emission patterns of the cube-bullseye

structure with two aforementioned circular grating periods (Figure 2d). It can be clearly seen that the optimal period results in better far-field directionality than the non-optimal one. This well-designed period was used in the sample fabrication.

In order to characterize the emission directionality and demonstrate the important role of the bullseye structure in the hybrid nanoantenna, a back focal plane imaging system was built to measure the angular fluorescent emission pattern of the sample in k -space. An objective with a NA of 0.9 (Olympus, MPlanFL N, 100 \times /0.9 BD, ∞ /0/FN26.5) was used for both the excitation and light collection (see Section 4). Hence, the maximum measurement range of the emission angle is 64° according to the NA. The k -space measurements of the emitted photons from quantum dots coupled to a single film-coupled nanocube, a cube-bullseye hybrid plasmonic antenna, and a single bullseye without the cube were performed (Figure 3a,c,e). The corresponding angular patterns are plotted in Figures 3b,d,f. It is shown that a single film-coupled nanocube results in an

emission pattern with a single lobe and broad emission angle range, because an in-plane magnetic dipole mode is formed in the gap on resonance.^[37,38] In comparison, the cube-bullseye hybrid plasmonic antenna generates a much narrower emission pattern with a single lobe and the emitted photons are mostly directed into the center of the k -space. The full-width at half-maximum (FWHM) of the emission pattern is in the range of $\pm 7^\circ$ around the normal direction. Compared with the gold bullseye structure without a nanocube, the presence of the nanocube in the bullseye structure does not influence the emission pattern significantly but largely enhances the emission intensity (Figure 1c).

To quantitatively describe the beaming effect of the emitted light, we introduce a parameter *directivity* from antenna theory,^[39] a figure of merit characterizing the radiation directionality,

$$D = \frac{2\pi}{\int_0^{\pi/2} \int_0^{2\pi} F(\theta, \varphi) \sin(\theta) d\theta d\varphi} \quad (2)$$

where $F(\theta, \varphi)$ is the normalized angular pattern defined by $F(\theta, \varphi) = S(\theta, \varphi) / \max\{S(\theta, \varphi)\}$ and $S(\theta, \varphi)$ is the pattern retrieved from simulation or measurement. Here, we only take the upper semi-spherical space into account because the emission transmitted through the 100 nm thick gold film can be neglected. According to the definition of Equation (2), the directivity is 1 (or equivalently 0 dB) when the radiation is a homogenous spherical wave (namely, no beaming effect); while the directivity is infinitely large, when the radiation is perfectly collimated. The measured directivity of our cube-bullseye hybrid plasmonic antenna is 16 dB, which has a good agreement with the calculated value of 17 dB. This value is much higher than 3.7 dB for the far-field emission of quantum dots coupled to a single film-coupled cube.

To further quantify the beaming effect of the proposed hybrid plasmonic antenna, another important quantity *collection efficiency* is studied, which is defined as the ratio of the energy emitted into a given NA to the total radiated energy. Efficient collection of the emitted photons using low NA optics, typically such as a fiber, is quite useful in practical applications of emission devices. For example, vertical-cavity surface-emitting laser has been successfully applied in optical communication partly because of the high coupling efficiency of its radiation into an optical fiber. The simulation results (Figure 4) show that the collection efficiency for the cube-bullseye hybrid antenna is much higher than that of the single film-coupled nanocube without bullseye. The calculated collection efficiency into an NA of 0.12, a typical value for a single-mode fiber, can reach 21% for the cube-bullseye hybrid antenna, which is much higher than 2.1% for a single film-coupled cube (see the inset in Figure 4). This shows that the existence of the bullseye structure enhances the collection efficiency into low NA by 10 times. Furthermore, an even higher collection efficiency of over 60% can be achieved using a multimode fiber with NA of 0.5. Figure 4 also shows the experimental collection efficiency η_m retrieved from Figure 3a,c, according to the following equation:

$$\eta_m(\text{NA}) = \frac{\iint_{\sqrt{k_x^2 + k_y^2}/k_0 < \text{NA}} I(k_x, k_y)}{\iint_{\sqrt{k_x^2 + k_y^2}/k_0 < 0.9} I(k_x, k_y)} \cdot \eta_{\text{theory}}(\text{NA} = 0.9) \quad (3)$$

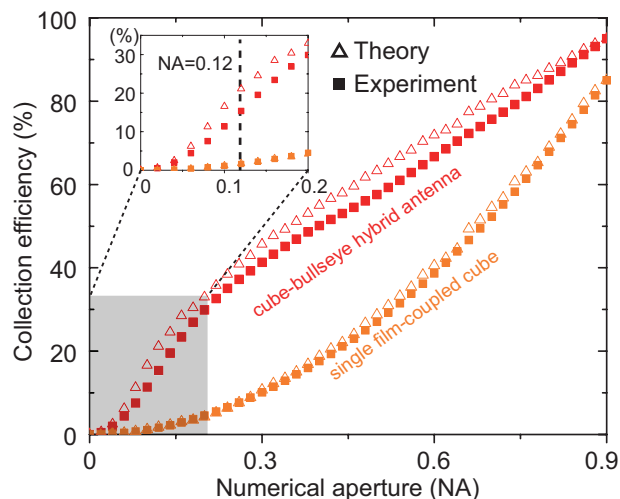


Figure 4. Dependence of the collection efficiency on NA. Theoretical (triangle) and experimental (square) collection efficiencies of the emission from quantum dots coupled to a single film-coupled nanocube (yellow) and a cube-bullseye hybrid plasmonic antenna (red) as a function of NA. Inset: collection efficiencies zoomed into the low NA range (gray area), where the NA of 0.12 is marked by a black dashed line.

where η_{theory} is the theoretical collection efficiency. The experimentally measured collection efficiencies into NAs of 0.12 and 0.5 exceed 16% and 50%, respectively. These efficiencies are the highest values reported so far to the best of our knowledge. The small deviation of the experimental values from the theoretical ones can be attributed to the fabrication imperfection of the samples and the broadband emission where not all wavelengths match the optimal period of the gold rings.

Compared with the previous studies on directional emission using the bullseye structure, our hybrid plasmonic antenna can achieve very large decay rate enhancement due to the existence of the vertical plasmonic nanogap in the center. The spontaneous emission is boosted according to the Fermi's golden rule because the quantum dots are placed in an environment with highly enhanced photon density of states. To verify that our structure can also enhance the decay rate while enhancing the directionality, time-resolved fluorescence of the quantum dots was measured. From Figure 5, it is clearly seen that there are significant differences of decay rates between the quantum dots on the glass substrate, on the bullseye antenna without cubes, and on the cube-bullseye hybrid plasmonic antenna. A single exponential decay dynamics with lifetime of 14 ns can be retrieved from the measured decay curve of quantum dots on glass. At the center of the gold bullseye structure without cubes, the quantum dots have a faster decay dynamics with a lifetime of 540 ps but the emission is inefficient due to the quenching by metal. For the quantum dots coupled to the cube-bullseye hybrid antenna, the fluorescence shows a significantly improved decay dynamics. The measured fluorescence response has a FWHM of 76 ps, which quite approaches the instrument response function (IRF) with a FWHM of 68 ps. A single exponential function featured decay with a lifetime of 33 ps is retrieved with the deconvolution from the IRF. Accordingly, a 424-fold total decay rate enhancement (14 ns/33 ps = 424) is obtained compared with quantum dots on glass as a con-

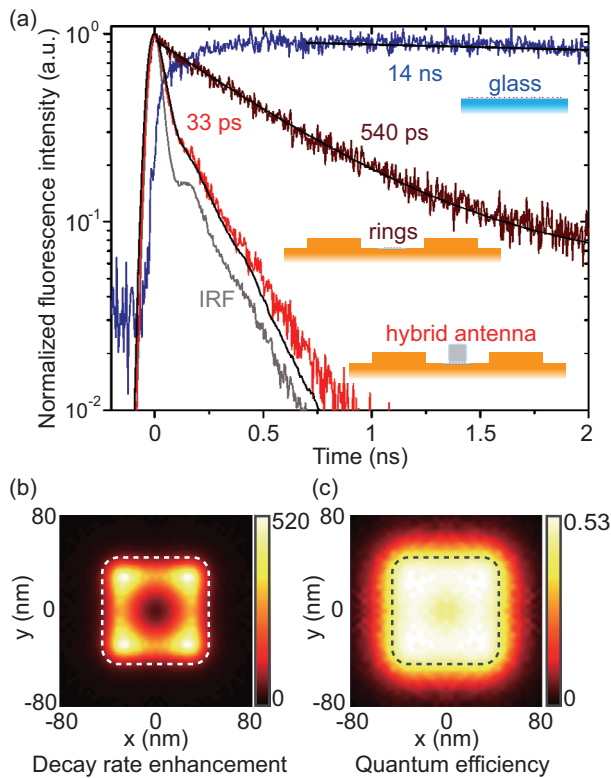


Figure 5. Enhanced spontaneous decay rate and quantum efficiency. a) Normalized time-resolved fluorescence of quantum dots coupled to the hybrid plasmonic antenna (red), compared with that of the quantum dots on a glass substrate (blue) and at the center of a gold bullseye structure (brown). The IRF of the system is shown in gray. A single exponential function is used to fit the decay curves of quantum dots on glass and on the gold bullseye structure. A single exponential function deconvoluted from the IRF is used to fit the decay dynamics of quantum dots coupled to the cube-bullseye hybrid antenna. All fitting curves are shown in black. b,c) Simulated total decay rate enhancement and quantum efficiency as a function of the dipole position in the nanogap between the nanocube and the ground gold film. The white and black dashed lines indicate the projection boundary of the nanocube.

control, which coincides well with the theoretical prediction of ≈ 500 (Figure 5b). Vertical dipole orientation was assumed in our simulations for its dominant contribution to the decay rate enhancement compared with the horizontal dipole orientation (Figure S5, Supporting Information). Such a high decay rate enhancement has not been reported in previous studies on bullseye unidirectional antennas, to the best of our knowledge. Large spontaneous emission enhancement is useful only if the quantum efficiency is high and the quantum efficiency can be indicated by the total intensity enhancement (Figure 1c). This large enhancement factor EF can be mainly attributed to the excitation rate enhancement in the nanogap, the quantum efficiency enhancement, and the collection efficiency enhancement according to

$$EF = \frac{\gamma_{\text{exc}}}{\gamma_{\text{exc}}^0} \cdot \frac{q}{q^0} \cdot \frac{\eta}{\eta^0} \quad (4)$$

where γ_{exc} is the excitation rate, whose enhancement equals to the square of electric field enhancement in the nanogap, that is,

$\gamma_{\text{exc}}/\gamma_{\text{exc}}^0 = |\mathbf{E}_{\text{exc}}|^2/|\mathbf{E}_{\text{exc}}^0|^2$, q is the quantum efficiency, η is the collection efficiency into a NA of 0.9 and the superscript “0” represents the sample of quantum dots on glass. The intrinsic quantum efficiency of quantum dots q^0 is 30%, measured in the water solution. Simulations show a PL enhancement factor of 200 resulting from the 26-fold average excitation rate enhancement, the 1.7-fold average quantum efficiency enhancement by embedding in the nanogap (Figure 5c) and the 4.5-fold collection efficiency enhancement (from 21% to 95%). The difference between the simulated EF of 200 and the experimental EF of 120 may originate from the non-uniform permittivity in the practical nanogap embedded with dense quantum dots. The improvement of quantum efficiency also leads to a larger enhancement in the radiative decay rate with a factor of over 700 calculated by $\gamma_r/\gamma_r^0 = (\gamma q)/(\gamma^0 q^0)$, where γ/γ^0 is the measured total decay rate enhancement of 424. Most importantly, in this single device, a high quantum efficiency, a high decay rate and a high directionality have been achieved simultaneously. If electrical pump and modulation can be applied to this hybrid antenna, it can potentially be developed as a nano-LED with high quantum efficiency, high fiber coupling efficiency, and high speed.

3. Conclusion

In summary, the proposed hybrid plasmonic antenna is a new platform combining the advantages of both the bullseye antenna and the plasmonic nanogap cavity. Compared with the single film-coupled nanocube without rings, the photon collection efficiencies of the cube-bullseye hybrid plasmonic antenna into a NA of 0.12 and a NA of 0.5 can be increased by 10 times and above 2 times, respectively. Meanwhile, a 424-fold enhancement of the spontaneous decay rate and a 121-fold enhancement of the total emission intensity have been demonstrated compared with quantum dots on glass as a control. The theoretically calculated quantum efficiency is as high as over 50%. This excellent performance is enabled by the SPPs decoupling occurred on the optimized circular periodic rings and by the large field enhancement in the well-controlled vertical nanogap created by the smooth surfaces of the colloiddally synthesized crystalline silver nanocube and the evaporated gold film. This hybrid plasmonic antenna can be used as a flexible platform for the enhancement of photon emission process with high quantum efficiency, high decay rate, and good directionality. Some new methods such as atomic force microscope tip pick-place technique,^[31] optical manipulation method^[40] and DNA self-assembly^[41] may be employed to establish this platform with more accurate control of the nanocube position and nanopatterning in large area. In the future, the proposed hybrid plasmonic antenna can be a good candidate to realize an energy efficient nano-LED with high modulation speed and high coupling efficiency into optical fibers or an ultrafast directional single photon source by integrating a single quantum emitter into the structure.

4. Experimental Section

Simulation: 3D full-wave simulations were performed based on finite element method using COMSOL Multiphysics 5.3a. The quantum dot was

modeled by a monochromatic electric dipole source with a vertical orientation and the emission frequency corresponding to the emission wavelength of 640 nm. An open source package was used to calculate the far-field emission pattern by retrieving the near field given by COMSOL and doing near to far field transformation.^[36] The final pattern results were obtained by averaging results from dipoles positioned beneath the four corners of the nanocube. The decay rate enhancement and quantum efficiencies can be retrieved by integrating the total radiative power and the Ohmic loss occurring in metals (see Supporting Information for details).

Sample Preparation: The sample preparation combines the electron-beam lithography (EBL) and the bottom-up self-assembly method. Gold align markers and concentric rings were first fabricated on the top of the gold ground film using the EBL and metal lift-off process. Then single PMMA holes with the diameter of 160 nm were created at the center of concentric rings after the second EBL process with required marker alignments. Monolayered colloidal quantum dots and colloidal silver nanocubes were then self-assembled on the top successively. Finally, quantum dots and silver nanocubes on the PMMA layer were lift-off by acetone. The quantum dots monolayer and single nanocubes dropped into the aforementioned PMMA holes were left. More detailed steps can be seen in Supporting Information.

Optical Setup and Measurements: Optical setup for measuring the fluorescent spectrum, the single nanocube scattering spectrum and the emission pattern was built based on a commercial microscope (Olympus, IX81) (see Supporting Information). Setup for measuring the fluorescence lifetime was built based on a separated microscope (Olympus, IX71). For the single nanocube scattering spectrum measurement, white light was obliquely shined on the sample through a dark field module (Olympus, U-MDF3) and a dark-field objective (Olympus, MPlanFL N, 100x/0.9 BD, $\infty/0$ /FN26.5) so that only scattered light can be collected by the objective and then imaged on the CCD camera in spectrometer (Renishaw, in-Via). The area of interest was selected by modifying the slit width and CCD pixels selection. For the fluorescent spectrum measurement, a collimated 532 nm continuous wave laser was used to excite the area of interest via the same objective and the fluorescence was also collected by the same objective and directed into the spectrometer. As for measuring the far-field emission pattern, a lens system was established to image the back focal plane of the objective on the sCMOS camera (Photometrics, Prime BS1). The back focal plane is the Fourier plane of the sample plane and thus includes the spatial frequency information, that is, k -space information, of the emitted light. Therefore, the angular intensity distribution can be retrieved by imaging this plane. The k -space was calibrated by a cross-grating (see Supporting Information for details). The time-resolved fluorescence measurement was performed based on a time-correlated single photon counting (TCSPC) module (PicoQuant, PicoHarp 300). A 532 nm picosecond pulsed diode laser was used to excite the sample, and a single photon avalanche diode was used to detect the emitted photons. In all time-resolved measurements, the detected photon-counting rate was kept at ≈ 3000 cps by adjusting the excitation power below 4 nW corresponding to the power density of 0.5 W cm^{-2} in order to avoid the biexciton emission.

Supporting Information

Supporting Information is available from the Wiley Online Library or from the author.

Acknowledgements

BB and HBS acknowledge the support by the National Key Research and Development Program of China and National Natural Science Foundation of China (NSFC) under Grants #2017YFF0206104, #61775113, #61960206 and #61590930. GY acknowledges the support by the China Scholarship Council (CSC No. 201606210320) and helpful discussion with Yuanmu Yang at the Department of Precision Instrument, Tsinghua Uni-

versity, Beijing. YN and HW acknowledge the support by the Ministry of Science and Technology of China and NSFC under Grants #2015CB932400 and #11774413.

Conflict of Interest

The authors declare no conflict of interest.

Keywords

directionality, optical antenna, plasmonics, Purcell effect, spontaneous emission

Received: June 22, 2019

Revised: November 7, 2019

Published online: February 11, 2020

- [1] P. Turchmann, N. Rotenberg, J. Renger, I. Harder, O. Lohse, T. Utikal, S. Gotzinger, V. Sandoghdar, *Nano Lett.* **2017**, *17*, 4941.
- [2] M. A. Baldo, D. F. O'Brien, Y. You, A. Shoustikov, S. Sibley, M. E. Thompson, S. R. Forrest, *Nature* **1998**, *395*, 151.
- [3] J. Yoneda, K. Takeda, T. Otsuka, T. Nakajima, M. R. Delbecq, G. Allison, T. Honda, T. Kodera, S. Oda, Y. Hoshi, N. Usami, K. M. Itoh, S. Tarucha, *Nat. Nanotechnol.* **2018**, *13*, 102.
- [4] R. M. Ma, R. F. Oulton, *Nat. Nanotechnol.* **2019**, *14*, 12.
- [5] A. Dreau, A. Tchegoratcheva, A. El Mahdaoui, C. Bonato, R. Hanson, *Phys. Rev. Appl.* **2018**, *9*, 064031.
- [6] T. Cai, S. Dutta, S. Aghaeimeibodi, Z. Yang, S. Nah, J. T. Fourkas, E. Waks, *Nano Lett.* **2017**, *17*, 6564.
- [7] M. S. Eggleston, S. B. Desai, K. Messer, S. A. Fortuna, S. Madhupathy, J. Xiao, X. Zhang, E. Yablonovitch, A. Javey, M. C. Wu, *ACS Photonics* **2018**, *5*, 2701.
- [8] G. Shambat, B. Ellis, A. Majumdar, J. Petykiewicz, M. A. Mayer, T. Sarmiento, J. Harris, E. E. Haller, J. Vuckovic, *Nat. Commun.* **2011**, *2*, 539.
- [9] I. Aharonovich, D. Englund, M. Toth, *Nat. Photonics* **2016**, *10*, 631.
- [10] K. L. Tsakmakidis, R. W. Boyd, E. Yablonovitch, X. Zhang, *Opt. Express* **2016**, *24*, 17916.
- [11] J. L. O'Brien, A. Furusawa, J. Vuckovic, *Nat. Photonics* **2009**, *3*, 687.
- [12] X. L. Chu, S. Gotzinger, V. Sandoghdar, *Nat. Photonics* **2017**, *11*, 58.
- [13] S. Huang, T. Ming, Y. Lin, X. Ling, Q. Ruan, T. Palacios, J. Wang, M. Dresselhaus, J. Kong, *Small* **2016**, *12*, 5190.
- [14] K. Matsuzaki, S. Vassant, H. W. Liu, A. Dutschke, B. Hoffmann, X. W. Chen, S. Christiansen, M. R. Buck, J. A. Hollingsworth, S. Gotzinger, V. Sandoghdar, *Sci. Rep.* **2017**, *7*, 42307.
- [15] G. M. Akselrod, C. Argyropoulos, T. B. Hoang, C. Ciraci, C. Fang, J. Huang, D. R. Smith, M. H. Mikkelsen, *Nat. Photonics* **2014**, *8*, 835.
- [16] E. Yablonovitch, *Phys. Rev. Lett.* **1987**, *58*, 2059.
- [17] A. G. Curto, G. Volpe, T. H. Taminiau, M. P. Kreuzer, R. Quidant, N. F. van Hulst, *Science* **2010**, *329*, 930.
- [18] M. Ramezani, A. Casadei, G. Grzela, F. Matteini, G. Tutuncuoglu, D. Ruffer, A. F. I. Morral, J. G. Rivas, *Nano Lett.* **2015**, *15*, 4889.
- [19] J. F. Ho, Y. H. Fu, Z. G. Dong, R. Paniagua-Dominguez, E. H. H. Koay, Y. F. Yu, V. Valuckas, A. I. Kuznetsov, J. K. W. Yang, *ACS Nano* **2018**, *12*, 8616.
- [20] I. M. Hancu, A. G. Curto, M. Castro-Lopez, M. Kuttge, N. F. van Hulst, *Nano Lett.* **2014**, *14*, 166.
- [21] H. Aouani, O. Mahboub, N. Bonod, E. Devaux, E. Popov, H. Rigneault, T. W. Ebbesen, J. Wenger, *Nano Lett.* **2011**, *11*, 637.
- [22] Y. C. Jun, K. C. Y. Huang, M. L. Brongersma, *Nat. Commun.* **2011**, *2*, 283.

- [23] H. Aouani, O. Mahboub, E. Devaux, H. Rigneault, T. W. Ebbesen, J. Wenger, *Nano Lett.* **2011**, *11*, 2400.
- [24] J. M. Yi, A. Cucho, E. Devaux, C. Genet, T. W. Ebbesen, *ACS Photonics* **2014**, *1*, 365.
- [25] L. Langguth, D. Punj, J. Wenger, A. F. Koenderink, *ACS Nano* **2013**, *7*, 8840.
- [26] Q. Li, H. Wei, H. Xu, *Nano Lett.* **2015**, *15*, 8181.
- [27] N. Livneh, M. G. Harats, S. Yochelis, Y. Paltiel, R. Rapaport, *ACS Photonics* **2015**, *2*, 1669.
- [28] N. Livneh, M. G. Harats, D. Istrati, H. S. Eisenberg, R. Rapaport, *Nano Lett.* **2016**, *16*, 2527.
- [29] M. G. Harats, N. Livneh, G. Zaiats, S. Yochelis, Y. Paltiel, E. Lifshitz, R. Rapaport, *Nano Lett.* **2014**, *14*, 5766.
- [30] J. T. Choy, I. Bulu, B. J. M. Hausmann, E. Janitz, I. C. Huang, M. Loncar, *Appl. Phys. Lett.* **2013**, *103*, 161101.
- [31] S. K. H. Andersen, S. Bogdanov, O. Makarova, Y. Xuan, M. Y. Shalaginov, A. Boltasseva, S. I. Bozhevolnyi, V. M. Shalaev, *ACS Photonics* **2018**, *5*, 692.
- [32] A. Kinkhabwala, Z. F. Yu, S. H. Fan, Y. Avlasevich, K. Mullen, W. E. Moerner, *Nat. Photonics* **2009**, *3*, 654.
- [33] D. Punj, R. Regmi, A. Devilez, R. Plauchu, S. B. Moparthi, B. Stout, N. Bonod, H. Rigneault, J. Wenger, *ACS Photonics* **2015**, *2*, 1099.
- [34] R. Chikkaraddy, B. de Nijs, F. Benz, S. J. Barrow, O. A. Scherman, E. Rosta, A. Demetriadou, P. Fox, O. Hess, J. J. Baumberg, *Nature* **2016**, *535*, 127.
- [35] T. B. Hoang, G. M. Akselrod, M. H. Mikkelsen, *Nano Lett.* **2016**, *16*, 270.
- [36] J. Yang, J. P. Hugonin, P. Lalanne, *ACS Photonics* **2016**, *3*, 395.
- [37] A. Moreau, C. Ciraci, J. J. Mock, R. T. Hill, Q. Wang, B. J. Wiley, A. Chilkoti, D. R. Smith, *Nature* **2012**, *492*, 86.
- [38] A. Rose, T. B. Hoang, F. McGuire, J. J. Mock, C. Ciraci, D. R. Smith, M. H. Mikkelsen, *Nano Lett.* **2014**, *14*, 4797.
- [39] C. A. Balanis, *Antenna Theory: Analysis and Design*. John Wiley & Sons, Hoboken, NJ **2005**.
- [40] L. Lin, M. Wang, X. Peng, E. N. Lissek, Z. Mao, L. Scarabelli, E. Adkins, S. Coskun, H. E. Unalan, B. A. Korgel, L. M. Liz-Marzán, E. L. Florin, Y. Zheng, *Nat. Photonics* **2018**, *12*, 195.
- [41] C. Y. Zheng, E. Palacios, W. Zhou, W. Hadibrata, L. Sun, Z. Huang, G. C. Schatz, K. Aydin, C. A. Mirkin, *Adv. Mater.* **2019**, *31*, 1904448.